# Modeling and Control of a Hybrid Reluctance Actuator with Tunable Remnant Magnetization

Dubey, Akshat; Ronaes, Endre; Hassan HosseinNia , S.

**DOI**
10.1016/j.ifacol.2025.10.155

**Publication date**
2025

**Document Version**
Final published version

**Published in**
IFAC-PapersOnline

Available online at www.sciencedirect.com

ScienceDirect

IFAC PapersOnline CONFERENCE PAPER ARCHIVE

IFAC PapersOnLine 59-17 (2025) 149–154

# Modeling and Control of a Hybrid Reluctance Actuator with Tunable Remnant Magnetization

**Akshat Dubey** * **Endre Ronaes** * **Hassan HosseinNia** *

* *Faculty of Precision and Microsystems Engineering (PME), Delft University of Technology, 2628CD Delft, Netherlands (email:{E.P.Ronaes, S.H.HosseinNiaKani}@tudelft.nl)*

**Abstract:** This paper explores the combination of a Hybrid Reluctance Actuator (HRA) with a Hybrid Tunable Magnet Actuator (HTMA) to realize a high bandwidth actuator that can generate low-frequency forces with greater efficiently. The HTMA allows desired forces to be sustained without continuous coil heating by manipulating the remnant magnetisation of an AlNiCo magnet. This enables the actuator to exert force through two modes of operation: by magnetisation of the Tunable AlNiCo Magnet (TM) or by inducing a proportionally force-dependent field. The second mode may furthermore be used to compensate for unwanted variations in forces during magnetisation. Although FEM analyses provide an understanding of the actuator behaviour in steady states, it is inefficient to integrate transient FEM models with accurate hysteresis models. Hence, firstly, an analytical framework is presented to determine the transient behaviour and the comparative energy efficiency of the two actuator modes. Then, a control strategy is presented for the operation of the combined actuator to track a reluctance force step reference. An experimental setup is designed and tested to validate the concept and control method.



*Keywords:* Hybrid Tunable Magnet Actuator, Hybrid Reluctance Actuator, Magnetic Equivalent Circuit, Hysteresis, Feedback control

## 1. INTRODUCTION

Thermal dissipation in actuated high-precision systems is increasingly forming a major hurdle to improving tracking accuracy and actuation bandwidth. Temperature variations in these systems can lead to significant thermal expansion of system components, resulting in changes that are difficult to predict and a deterioration of the system performance [Lomonova (2010)]. While electromagnetic (EM) actuators offer precise and high non-contact positioning forces in applications like photolithography and metrology, Joule heating of magnetising coils is an inherent issue [Hüfner et al. (2017)].

The higher force density of Reluctance Actuators (RA), is increasingly driving their adoption as substitutes in traditionally Lorentz-coil actuated systems [Vrijsen et al. (2010), Cigarini et al. (2019)]. A shift that is supported by the development of Hybrid-RA (HRA) topologies providing a linear motor constant, and the addition of more advanced control methods [Schmidt et al. (2020), Ito et al. (2019a)], enabling their use in applications like high-precision scanning motion systems [Ito et al. (2019b)] and fast steering mirrors [Csencsics et al. (2019)]. However, these actuators demand continuous current supply to sustain actuation forces, resulting in accumulated Joule heating leading to compromised system performance.

To address the issue of sustained Joule heating under quasi-static loading conditions, Electro-Permanent Magnet Actuators Knaian (2010) and Tunable Magnet Actuators (TMAs) Viëtor (2018) utilise the concept of in-situ magnetisation of a Low Coercive Force (LCF) Permanent Magnets (PMs) to generate a constant magnetic flux in an RA without continuously powering the magnetising coil. The HRA design – introducing biasing flux from High Coercive Force (HCF) PMs – is utilised in Hoekwater et al. (2023) to linearise the motor constant of a TMA. The resulting actuator, known as a Hybrid TMA (HTMA) generates a quasi-static reluctance force that varies linearly with the remnant magnetisation state of the AlNiCo tunable magnet.

The HTMA only maintains its efficiency advantage over HRAs at low frequencies and introduces high-frequency dynamics in the transition between remnant magnetisation states. This issue is solved in [Pechhacker et al. (2024)] by integrating a Lorentz coil actuator that acts in parallel. This paper proposes a more compact solution through a hybrid design that combines the ability to induce and linearly control high magnetic fluxes with low currents and the option of producing sustained fluxes through the manipulation of permanent magnetisation states. Effectively, combining both features of an HRA and the HTMA in a single stator core. Combined control of the two inputs allows the actuator to attain higher energy efficiency at lower frequencies, as compared to other HRAs, and the


10.1016/j.ifacol.2025.10.155

ability to sustain a force over an indefinite period of time without dissipating heat. The latter part of this paper presents a controller design

Section 2 introduces the conceptual design of the combined actuator. Section 3 presents an analysis of the energy efficiency and actuation force through the design of an equivalent circuit model. A control algorithm is proposed in Section 4 and is implemented on a test setup in Section 5.

## 2. SYSTEM DESCRIPTION

The proposed actuator comprises two magnetic flux loops controlled by separate voltage sources. The schematic representation in Fig. 3 illustrates the individual loops, highlighted in red and blue, flowing through the left and right side of the mover, respectively. For brevity, these are referred to as the Tunable Magnet (TM), and Reluctance Actuator (RA) loops, respectively. The TM and RA flux paths sum together with the flux sustained by the two Neodymium PMs (*green*). The PMs furthermore serve the additional purpose of roughly isolating the TM and RA loops, due to their high reluctance.

The rectangular mover experiences an attractive reluctance force toward each of the four poles. The magnitude of these forces is proportional to the square of the total magnetic flux flowing through each respective air gap. The overall force $F$ acting on the mover is therefore the summation of these attractive forces. Assuming the magnetic field lines are perpendicular to the surface of the mover, the total force acting on it is obtained from the Maxwell stress tensor [Schmidt et al. (2020)] as

$$F = \frac{1}{2A_g\mu_0}\left[(\phi_{TM}+\phi_{PM})^2-(\phi_{TM}-\phi_{PM})^2 + (\phi_{RA}+\phi_{PM})^2-(\phi_{RA}-\phi_{PM})^2\right], \quad (1)$$

Where $A_g$ is the cross-sectional area of the air-gaps and $\mu_0$ is the magnetic permeability of air ($\mu_0 \approx 4\pi \cdot 10^{-7}$ $\mathrm{H\,m^{-1}}$). The magnetic fluxes $\phi_{TM}$, $\phi_{RA}$ and $\phi_{PM}$ are induced by the TM, the RA coil and the neodymium magnet, respectively, as denoted in Fig. 3. Thus, provided the spacing between the poles and the mover is equal and the loops illustrated in Fig. 3 are indeed isolated, a variation of $\phi_{TM}$ or $\phi_{RA}$ results in a proportional change in the force acting on the mover,

$$F = \frac{\phi_{PM}}{\mu_0 A}(\phi_{TM}+\phi_{RA}), \quad (2)$$

Naturally, the flux loops cannot be insulated within these regions of the actuator. Furthermore, positionally dependent flux leakage around the air-gaps will result in a reduction in the force. A common practice, especially in voice coil actuators, is to multiply the force estimation (1) with a flux leakage constant, which may vary from 0.75 to as much as 0.25 [Cigarini et al. (2019)]. Other solutions, such as the addition of fringing flux paths may provide a better estimation by considering the influence of the mover position. However, the primary objective is to study the attainable energy efficiency by simultaneous control of

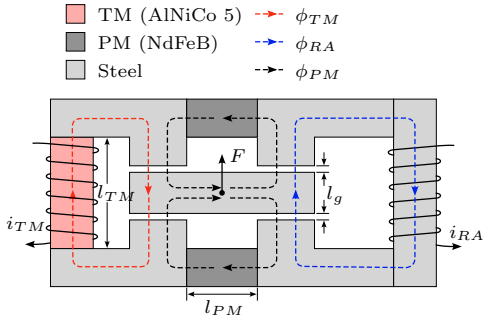


(a)

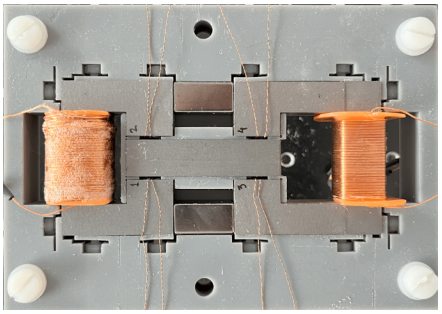

(b)

Fig. 1. Hybrid tunable magnet actuator: (a) schematic of the magnetic flux paths (b) photograph of the experimental setup.

magnetic fluxes $\phi_{TM}$ and $\phi_{RA}$. The chosen design allows the magnetic fluxes to be measured and controlled, but cannot function as an actuator as the mover has to be constrained from the torsional forces. Modifications can be made to the proposed design, introducing symmetry and cancelling out such forces.

## 3. CORE AND COIL LOSSES

Improving the energy efficiency of the system presents a trade-off between copper loss (Joule heating) and core losses (mostly from hysteresis losses in the *Tunable Magnet*). As a proportion of the total volume of copper, coil losses are reduced by minimising the current density $J$ in the windings and the time-period $T$ over which it is sustained (3). The energy density stored within the magnetic cores is determined by integrating the local magnetic field intensity $H$ over the change in the local flux density $B$ (3).

$$W_{coil} = \int_0^T \frac{J^2}{\sigma} dt \quad (3)$$

$$W_{core} = \int_0^T H \cdot \frac{dB}{dt} dt \quad (4)$$

Magnetising the TM necessitates a spike in the average field across the magnet, at times nearing $130\,\mathrm{kA\,m^{-1}}$ to fully saturating the material. Provided the magnet in Fig. 3 has a length of 30 mm and is magnetised by a coil with 405 turns of wire, a 9.6 A current is required to saturate the magnet.

To determine the energy losses during this period, the transient evolution of the coil current $i$ during the appli-

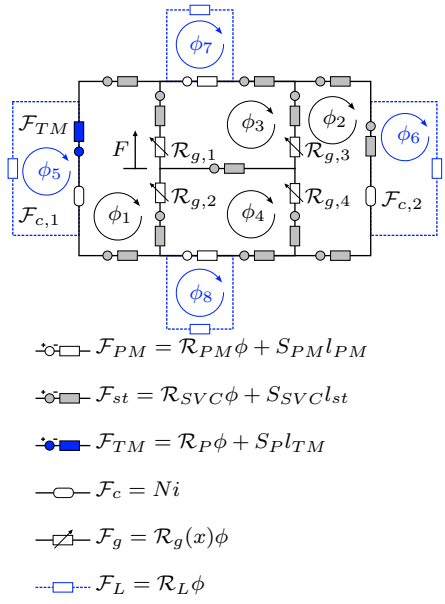


Fig. 2. A magnetic equivalent model of the actuator. Ferromagnetic components are considered as a series connection of a magnetic reluctance $\mathcal{R}$ and a MMF-source (the values of which are iteratively updated to reflect the nonlinear flux-field relation in respective elements). Flux fringing paths – illustrated in blue – are added around the magnets.

cation of a voltage $V$ (5) must be known. The derivation of which is complicated by that the inductive resistance depends on the nonlinear and history-dependent variation of the magnetic flux $\phi$ with respect to the induced magnetomotive force (MMF) $\mathcal{F}$.

$$V = iR + N\frac{d\phi}{dt} \tag{5}$$

A Preisach model, which can be tuned to provide an accurate phenomenological description of magnetic hysteresis, is chosen to model the hysteresis in the AlNiCo magnet [Mayergoyz (1986)]. In comparison, magnetic hysteresis in the steel cores is negligible, but saturation is considered by a single value curve (SVC) describing the approximate anhysteretic $BH$-relation in the laminated steel (Fig. 3). As in [Ceylan et al. (2023)], the contribution of classical eddy-current and excess field losses are added based on an Euler backward approximation of the rate of change in magnetic flux.

At any point in time, the MMF can be linearly described as function of $i$ and $\phi$ (6). Wherein, the MMF and the reluctance $\mathcal{R}$ must be iteratively updated such as to conform with the nonlinear flux-field relation in a given component.

$$\mathcal{F} = \mathcal{R}\phi + Ni \tag{6}$$

Consequently, the magnetic equivalent circuit in Fig. 3 is constructed where segments of the actuator through which flux flows are defined as lumped components. For each lumped element, a linear equation (7) is interpolated relating the inductive field $H$ and the flux density $B$.

$$H = \mu^{-1}B + H_c \tag{7}$$

where $\mu$ is the magnetic *permeabiliity* and $H_c$ the coercive-field. The reluctance $\mathcal{R}$ (8) of and MMF (9) across a given element can be determined from the derived values of $\mu$ and $H_c$, and provided the flux path length $l$ and cross-sectional area $A$,

$$\mathcal{R} = \frac{l}{\mu A} \tag{8}$$

$$\mathcal{F}^{BH} = H_c l \tag{9}$$

In *fixed-point* (FP) iterations $\mathcal{R}$ and $\mathcal{F}^{BH}$ are derived from the nonlinear models of the BH-relation in the steel cores and the magnets and substituted into (6). The resulting states of $i$ in the electrical circuits and $\phi$ in the coupled magnetic circuit (Fig. 3), are solved at time intervals $\Delta t$ by a Euler backward-approximation of (5) and (6):

$$\begin{bmatrix}\boldsymbol{\phi}_k \\ \boldsymbol{i}_k\end{bmatrix} = \begin{bmatrix}\boldsymbol{R}_{k-1} & -\mathbf{N} \\ \Delta t^{-1}\mathbf{N}^T & \mathbf{R}\end{bmatrix}^{-1}\begin{bmatrix}-\boldsymbol{F}^{BH}_{k-1} \\ \boldsymbol{V}_{S,k} + \Delta t^{-1}\mathbf{N}\boldsymbol{\phi}_{k-1}\end{bmatrix} \tag{10}$$

where at FP-iteration $k$, $\boldsymbol{\phi}_k$ is a vector of the fluxes $[\phi_1, \ldots, \phi_8]^T_k$ in each loop illustrated in Fig. 3, $\boldsymbol{i}_k$ contains the current in each coil $[i_{TM}, i_{RA}]^T_k$, and the input voltages to the coils $[V_{TM}, V_{RA}]^T_k$ are defined in $\mathbf{V}_k$. The submatrix $\boldsymbol{R}_{k-1}$ consists of the reluctances of the lumped elements and $\boldsymbol{F}$ is a vector of the MMF throughout each loop (11). $\mathbf{R}$ contains the electrical resistances of the TM and RA coils, and $\mathbf{N}$ the number of windings (12),

$$\boldsymbol{R} = \begin{bmatrix}\mathcal{R}_{11} & \ldots & -\mathcal{R}_{18} \\ \vdots & \ddots & \vdots \\ -\mathcal{R}_{18} & \ldots & \mathcal{R}_{88}\end{bmatrix}, \qquad \boldsymbol{F} = \begin{bmatrix}\mathcal{F}_1 \\ \vdots \\ \mathcal{F}_8\end{bmatrix}, \tag{11}$$

$$\mathbf{R} = \begin{bmatrix}R_{TM} & 0 \\ 0 & R_{RA}\end{bmatrix}, \qquad \mathbf{N} = \begin{bmatrix}N_{TM} \\ N_{RA}\end{bmatrix} \tag{12}$$

In $\boldsymbol{R}$ the main diagonal of terms $\mathcal{R}_{11}, \ldots, \mathcal{R}_{88}$ are the sum of the reluctances in each loop and the cross terms represent the sum of reluctances intersecting two loops. The resulting value of $\phi_k$ is inserted in the nonlinear flux-field relations of the respective elements, providing a new updated value of $\mathcal{R}$ and $\mathcal{F}^{BH}$ of each component. This iterative process is repeated until the solutions $[\boldsymbol{\phi}_k, \boldsymbol{i}_k]^T$ and $[\boldsymbol{\phi}_{k-1}, \boldsymbol{i}_{k-1}]^T$ have converged within an acceptable error.

The energy losses are determined from (3) and (4), by numerical integration. Fig 3 shows the calculated energy losses when providing a sustained force by either magnetising the TM (*blue*) or providing a sustained field input through the RA coil (*red*). At 9 ms the joule heating from the RA-coil exceeds the core and coil losses produced by the magnetisation of the TM. Depending on the amplitude of the desired force, this 'break-even' point changes. It is for example more efficient for the RA-coil to sustain small variations in flux from 0 T over a longer duration compared to the field required to magnetise the TM. The 'break-even' time reduces when considering fluxes that are further

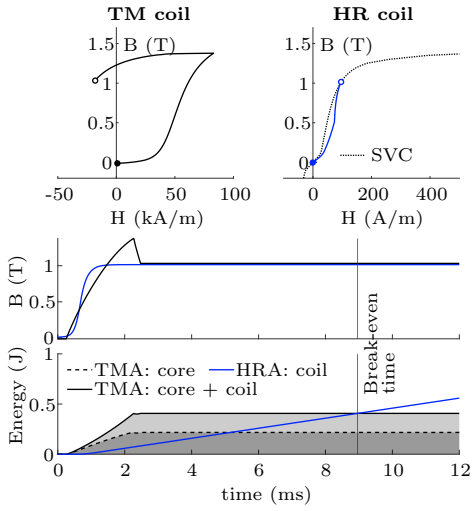


Fig. 3. *Breaking even:* comparison of energy losses over time by inducing a sustained flux by either using the TM coil to magnetise the TM (resulting in the change of its $BH$-state shown in the *upper left-hand corner*) or by supplying a continuous current through the RA coil (maintaining the $BH$-field indicated by the blue circle in the *upper right-hand corner*). At 9 ms the Joule heating from the RA-coil exceeds the core and coil losses produced by the magnetisation of the TM.

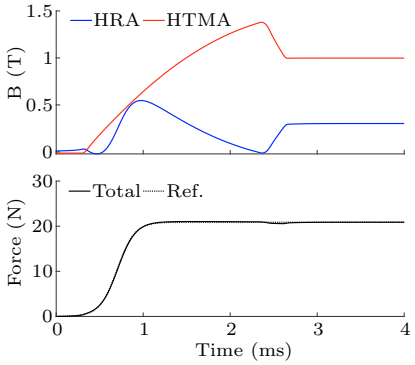


Fig. 4. Combination of RA and TM voltage inputs to generate a smooth step

away from 0 T, making it more desirable to manipulate the magnetisation state.

As illustrated in Fig. 3, reaching a given remnant magnetisation state requires the TM to be magnetised to a higher level of magnetic flux (1.4 T), before reducing the input field. The reluctance force (2) consequently overshoots the reference by a proportional magnitude. To mitigate this, a field input may be provided to the RA-coil, to generate a compensating force. Fig. 4 shows how flux density through the RA-coil can be controlled so that the total resulting force from the two modes of the actuator tracks a smooth step increase, while the TM is tuned from 0 to 1 T.

Altogether, the model is simplified and inadequate for generating an accurate estimation of actuation forces, it provides a good prediction of the point at which tuning the remnant magnetisation of the TM is the most energy-efficient alternative. This forms the basis for determining a control algorithm that efficiently combines both modes of actuation: magnetising the TM or generating a field through the low-reluctance path(s). Various parameters, like the distribution of the Preisach density and the reluctance to flux leakage around the magnets and coils, can be tuned to improve the agreement of the model with experimental measurements.

## 4. CONTROLLER DESIGN

A feedback control strategy is presented in Fig. 5 to operate the combined actuator [1].

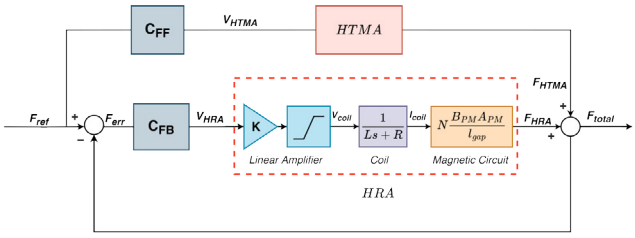


Fig. 5. Feedback control strategy

This strategy aims to use the HRA to provide a compensating force against the HTMA force overshoot, as exemplified in Fig. 8. Hence, the HRA is controlled in a negative feedback loop where the HTMA force acts as an output disturbance. The $C_{FF}$ block represents the feedforward control of the HTMA using one of the control strategies developed in [Ronaes et al. (2023)]. $C_{FB}$ represents the P-I feedback controller designed for the HRA.

The HRA block in the control loop consists of the linear amplifier gain $K = 3$ and saturation ($\pm 5V$), the *coil* transfer function, and the HRA motor constant, which is proportionally dependent on the biasing flux of the HCF PMs $B_{PM}$.

### *4.1 Feedback Controller Design*

The feedback controller design requires accurate knowledge of the HRA plant. Hence, the transfer function of a first-order system with a time delay is fitted to that of the plant measured using closed-loop system identification. The fitted analytical transfer function takes the following form:

$$G_{fit}(s) = \frac{5.2685 \times e^{-7.5\times10^{-5}s}}{6.5 \times 10^{-4}s + 2.5} \tag{13}$$

Additionally, to ensure robustness against instability in a closed-loop system, following conditions for the Gain Margin (GM), Phase Margin (PM), and Modulus Margin (MM) of the system are set:

$$GM \geq 6dB; PM \geq 30°; MM \leq 6dB \tag{14}$$

Considering the response of the closed loop system starts to deteriorate at frequencies higher than 3kHz, the controller is initially designed for a system bandwidth close to

[1] The position of the mover resulting from the reluctance force of the actuators is of greater interest in motion systems. However, since this paper considers a fixed mover for reasons discussed in Section 2, the total reluctance force is considered as the output of the system.

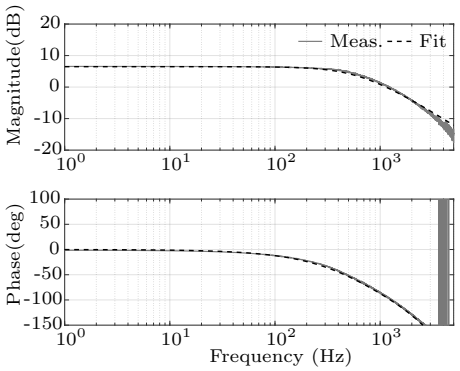


Fig. 6. Measured and Fitted HRA Plants

this frequency and then tuned until the stability requirements are met experimentally. The Open Loop ($L$), Complimentary Sensitivity ($TS$), and Sensitivity ($S$) transfer functions of the designed and measured systems are shown in Fig. 7. The controller parameters and achieved stability margins are presented in Table 1

Table 1. Controller parameters and stability margins

| Property | Value | Comment |
|---|---|---|
| $C_{FB}$ | $K_p(1+\frac{\omega_i}{s})$ | PI controller |
| $K_p$ | 1.5 | Proportional gain |
| $\omega_i$ | 628.32 | Integrator frequency in rad/s |
| $GM$ | 7.5 dB | Gain margin |
| $PM$ | 56° | Phase margin |
| $MM$ | 3.9 dB | Modulus margin |

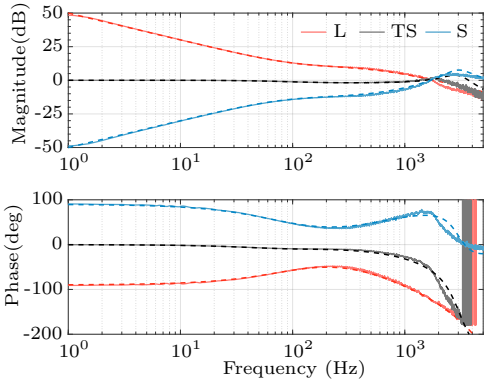


Fig. 7. Measured and Designed open-loop transfer function $L$, complimentary sensitivity $TS$, and sensitivity $S$ - Solid and dashed lines represent experimentally identified and mathematically derived magnitude and phase thereof

## 5. VALIDATION

To test the HTMA force overshoot compensation achieved using the presented control strategy, the combined actuator is made to track a single step of 0.5N. When only the HTMA is used to track this reference, the force overshoots to 3.696N.

To test performance of the combined actuator, the 0.5N reference is first tracked with the HRA while the TM remains demagnetised. Then, a magnetization pulse is input to the HTMA to generate the same force. As the feedback error increases with the HTMA force, the HRA generates an opposing force to reject the disturbance caused by HTMA force.

A Simulink model is developed to simulate this scenario. The stepping time of the Simulink solver is set at 20$\mu$s, to match the loop rate at which the feedback control runs on the NI-LabVIEW compactRIO-9039 Real-Time controller in the experimental setup. The plant and controller transfer functions are discretised at this rate using the *tustin* method and the measured HTMA force is used as the output disturbance.

A comparison between the simulation and its experimental validation is shown in Fig. 8. The HRA effectively compensates the HTMA force overshoot, resulting in ∼61.2% less overshoot compared to HTMA force alone, with the total force peaking at 1.737N.

The Maximum Absolute Error (MaxAE) of the total force (Table 2) is evaluated to quantify the force overshoot compensation achieved by the HRA.

Table 2. Force error evaluation

| Platform | MaxAE |
|---|---|
| Simulation | 1.2378 N |
| Experiment | 1.2384 N |

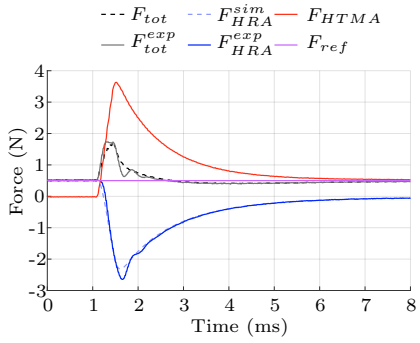


Fig. 8. Combined actuator operation - the force overshoot from the HTMA is compensated by the HRA to enable faster reference tracking

The currents in magnetizing coils of both, the HTMA and the HRA decay to zero once the combined actuator tracks the force reference, showing that a static force is generated without continuous energy expenditure (Fig. 9).

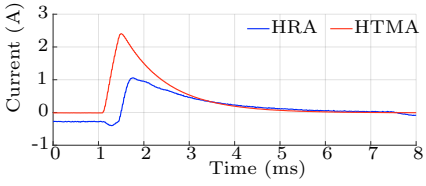


Fig. 9. Current in HTMA and HRA magnetising coils. Reduces to 0 A at the end of the run period.

## 6. CONCLUSION

A novel actuator design that integrates a Tunable Magnet in a Hybrid Reluctance actuator is proposed in this paper, to reduce energy dissipation from Joule heating at lower

actuation frequencies. As a result, the actuator exhibits two modes of actuation, whereby one generates a force by inducing a field through a low-reluctance path – as in traditional reluctance actuators – and another produces a force by tuning the remnant magnetisation of a magnet. By manipulating of magnetisation state of the tunable magnet overall heating can be reduced during sustained or slowly varying forces. A lumped circuit model is designed to determine the comparative energy dissipation in the actuator's two modes of operation, incorporating the hysteresis in the tunable magnet through a Preisach model.

A feedback control strategy is devised to operate the two parts of the actuator simultaneously to achieve faster and more accurate reference tracking. This strategy, along with the actuator design, is validated experimentally. Demonstrating that the combination of the two actuators results in greater than 60% reduction in overshoot in comparison to a Tunable Magnet Actuator alone. Ultimately, this combines the speed advantage of reluctance actuators with the sustained force advantage of Tunable Magnet Actuators.

Future work includes the construction of a short-stroke actuator based on the concept and model described in this paper. Additional work will be done to develop a closed-loop position control algorithm that employs both modes of actuation in an energy-efficient way. The tracking performance of the reluctance actuator is limited by the maximum supply of the power electronics, which must be improved for use beyond proof of principle.

## ACKNOWLEDGEMENTS

This work has been supported by the Dutch Research Council (NWO) Open Technology Program (OTP) for Applied and Technical Science (ATS) under project Beat the heat with number 19930.

## Appendix A. ACTUATOR PARAMETERS

Table A.1. Actuator Parameters

| Property | Value | Comment |
|---|---|---|
| **AlNiCo Permanent Magnet** | | |
| $l_{TM}$ | 30 mm | Length |
| $A_{TM}$ | 10x10 mm$^2$ | Cross section |
| **NdFeB Permanent Magnet** | | |
| $l_{PM}$ | 20 mm | Length |
| $A_{PM}$ | 10x10 mm$^2$ | Cross section |
| $B_{r,PM}$ | 1.38 T | Remnant Flux Density |
| **Air Gap** | | |
| $l_g$ | 1.25 mm | Length |
| $A_g$ | 15x10 mm$^2$ | Cross Section |
| **HTMA Coil** | | |
| $V_{max,HTMA}$ | 30 | Maximum voltage |
| $N_{TM}$ | 405 | Number of turns |
| **HRA Coil** | | |
| $V_{max,HRA}$ | 5 | Maximum voltage |
| $N_{RA}$ | 50 | Number of turns |

## REFERENCES

Ceylan, D., Zeinali, R., Daniel, B., Boynov, K., and Lomonova, E. (2023). A novel modeling technique via coupled magnetic equivalent circuit with vector hysteresis characteristics of laminated steels. *IEEE Transactions no Industry Applications*, 59(2), 1481–1491.

Cigarini, F., Ito, S., Troppmair, S., and Schitter, S. (2019). Comparative finite element analysis of a voice coil actuator and a hybrid reluctance actuator. volume 138, 1–8.

Csencsics, E., Schlarp, J., Schopf, T., and Schitter, G. (2019). Compact high performance hybrid reluctance actuated fast steering mirror system. *Mechatronics*, 62, 102251.

Hoekwater, W.B., Ronaes, E., and HosseinNia, H. (2023). Hybrid tunable magnet actuator: Design of a linearized force-flux tunable magnet actuator. *IEEE Transactions on Industrial Electronics*.

Hüfner, T., Radler, O., Ströhla, T., Sattel, T., Wesselingh, J., Vogler, A., and Eicher, D. (2017). A note on electromagnetic gravity compensation actuators based on soft electro-permanent magnets for adjustable reluctance force. In *Proceedings of the 17th International Conference of the European Society for Precision Engineering and Nanotechnology*, 149–150.

Ito, S., Cigarini, F., and Schitter, G. (2019a). Flux-controlled hybrid reluctance actuator for high-precision scanning motion. *IEEE Transactions on Industrial Electronics*, 67(11), 9593–9600.

Ito, S., Troppmair, S., Cigarini, F., and Schitter, G. (2019b). High-speed scanner with nanometer resolution using a hybrid reluctance force actuator. *IEEJ Journal of Industry Applications*, 8(2), 170–176.

Knaian, A.N. (2010). *Electropermanent magnetic connectors and actuators : devices and their application in programmable matter*. Ph.D. thesis, Massachusetts Institute of Technology.

Lomonova, E.A. (2010). Advanced actuation systems — state of the art: Fundamental and applied research. In *2010 International Conference on Electrical Machines and Systems*, 13–24.

Mayergoyz, I. (1986). Mathematical models of hysteresis. *IEEE Transactions on magnetics*, 22(5), 603–608.

Pechhacker, A., Wertjanz, D., Csencsics, E., and Schitter, G. (2024). Integrated electropermanent actuator with adaptable zero power gravity compensation. *IEEE Transactions on Industrial Electronics*, 71(5), 5055–5062.

Ronaes, E., Hunt, A., and HosseinNia, H. (2023). Remnant magnetisation state control for positioning of a hybrid tunable magnet actuator. *Energies*, 16(12), 4548.

Schmidt, R., Schitter, G., and Rankers, A. (2020). *The Design of High Performance Mechatronics - 3rd Revised Edition: High-Tech Functionality by Multidisciplinary System Integration*. IOS Press.

Viëtor, S. (2018). Tunable magnets: Modeling and validation for dynamic and precision applications.

Vrijsen, N., Jansen, J., and Lomonova, E. (2010). Comparison of linear voice coil and reluctance actuators for high-precision applications. In *Proceedings of 14th International Power Electronics and Motion Control Conference EPE-PEMC 2010*, S3–29. IEEE.